Summary of PhD Thesis
Radio and Submm Studies of Active Galactic Nuclei

by
Avinanda Chakraborty
Registration Number: R-18RS209210247

Date of Registration: 17.5.2021

Supervisor: Dr. Suchetana Chatterjee
School of Astrophysics

Presidency University, Kolkata, India - 700073

Abstract

It has been inferred from large unbiased samples of quasars that 10%-15% of all quasars are radio-loud (RL). Using the quasar catalog from the Sloan Digital Sky Survey (SDSS), we show that the radio-loud fraction (RLF) for high broad line (HBL) quasars, containing Hβ and MgII FWHM greater than $15,000$ km s^{-1}, is $> 40\%$. We find bolometric and optical continuum luminosity of the RL quasars are higher while there is no significant difference in other fundamental properties between the RL and radio-quiet (RQ) populations in our sample. By comparing them with the non-HBL Hβ broad emission line quasars, we find that the HBL sources have the lowest Eddington ratios in addition to having a very high RLF. This is consistent with the theories of jet formation, in which jets are launched from low Eddington ratio systems. We find a connection between a brighter accretion disk and a prominent jet and find that the [O III] narrow emission line is stronger in the RL compared to RQ quasars in our HBL sample, which is consistent with previous findings in the literature, and is likely to be caused by the interaction of the narrow line gas with the jet.

To probe the energetic outflows from quasars that are responsible for heating the intergalactic medium we model the thermal Sunyaev-Zeldovich (SZ) effect from quasar outflows. We use the GIZMO meshless finite mass hydrodynamic cosmological simulation SIMBA (Davé et al. 2019), which includes different prescriptions for quasar feedback. From these theoretical simulations, we perform mock observations of the Atacama Large Millimeter Array (ALMA) in four bands (320 GHz, 135 GHZ, 100 GHz and 42 GHz) to characterize the feasibility of direct detection of the quasar SZ signal. Our results show that for all the systems we get an enhancement of the SZ signal, when there is radiative feedback, while the signal gets suppressed when the jet mode of feedback is introduced in the simulations. Our mock ALMA maps reveal that, with the current prescription of jet feedback, the signal goes below the detection threshold of ALMA. We also find that the signal is higher for high redshift systems, making it possible for ALMA and cross SZ-X-ray studies to disentangle the varying modes of quasar feedback and their relative importance in the cosmological context. We further investigate the host galaxy properties of radio loud and radio quiet quasars by modeling their spectral energy distribution. Our preliminary studies show that there is no significant difference in the host galaxy properties between radio loud and radio quiet quasars.

Contents

1 Introduction **4**

1.1 Classification of Active Galactic Nuclei 4

1.2 The Quasar Galaxy Co-Evolution 5

1.3 Host Galaxy Property Analysis 6

1.4 Summary of Thesis Work 6

2 Radio Dichotomy Analysis of Broad Emission Line Quasars **7**

2.1 Data Sets 8

2.2 High Broad Emission Line (HBL) Hβ Sample 10

2.3 Low Broad Emission Line (LBL) Hβ Sample 12

2.4 Very Broad Emission Line (VBL) MgII Sample 12

3 The Sunyaev-Zeldovich Effect from Quasar Feedback **13**

3.1 Modelling Feedback Modes from Active Galactic Nuclei 13

3.2 Construction of Sunyaev-Zeldovich Maps 14

3.3 Theoretical Sunyaev-Zeldovich Maps 15

3.4 Mock Observational SZ Maps 17

4 Spectral Energy Distribution Analysis of the Quasar Sample **17**

4.1 The Code: X-CIGALE 17

5 Summary of Results and Future Plans **19**

1. Introduction

In our universe a small fraction ($\sim 10\%$) of galaxies has a compact central region with high luminosity ($L \sim 10^{44-48}$ ergs/s) that emits radiation comparable to or sometimes higher than the radiation emitted by the rest of the galaxy. Such galaxies are called 'active galactic nucleus' (AGN). AGN often produce variable emissions that can extend from radio to γ-rays and show strong broad emission line spectra. The term AGN refers to the existence of energetic phenomena in the central region of galaxies. The structure of the compact region and the signatures in their spectrum is used as the classification scheme for AGN. Quasars are the brightest among all AGN (Schmidt 1963), where the nuclear source is at least 100 times brighter than the stars in their host galaxies. In the first observations, quasars appeared as star-like objects, because in a quasar, only the star-like nuclear source is seen at very large distances and light from the surrounding galaxy is lost in the glare of the nucleus. Hence, the name 'quasi-stellar'.

1.1. Classification of Active Galactic Nuclei

As the physics underlying the AGN phenomenon is not yet understood properly, the classification of AGN tends to be rather subjective. Undoubtedly, more than the fundamental differences between the various types of AGN, the differences we see between the various types are due to the way we observe them. Although many quasars were discovered more than 40 years back because of their strong radio emission, it soon became evident that the majority of quasars are actually radio-quiet. But radio-quiet did not imply radio-silent, infact the two radio sub-classes can be termed as 'radio-strong' and 'radio-weak'. It is now known that only about 10 - 15% of quasars are radio-loud.

Quasars that are radio quiet closely resemble the 10% that are radio loud. The physical origin of this radio-dichotomy is yet to be understood. Studies tried to reveal the apparent connection between black hole mass and radio loudness, reported first by Franceschini et al. (1998) and confirmed in subsequent studies (e.g., McLure et al. 1999; Lacy et al. 2001; McLure & Jarvis 2004). However, the dichotomy has also been studied in the context of accretion rates (e.g., Sikora et al. 2007; Hamilton 2010), host galaxy properties (e.g., Sikora et al. 2007; Lagos et al. 2009; Kimball et al. 2011), as well as black hole (BH) spin (e.g., Blandford & Znajek 1977; Blandford 1990; Garofalo et al. 2010). It has been proposed that there may be multiple mechanisms responsible for powering the radio emission, for example it may come from a combination of small-scale jets as well as star forming regions (Cirasuolo et al. 2003b; Sabater et al. 2019). In the cosmological context, the role of galaxy mergers and host dark matter halos in the radio dichotomy has also been discussed (e.g., Hughes & Blandford 2003; Shen et al. 2007;

Hickox et al. 2009; Lagos et al. 2009; Garofalo et al. 2010; Hamilton 2010).

1.2. The Quasar Galaxy Co-Evolution

Since the last few decades, it has been established that supermassive black holes (SMBH) residing at the centers of galaxies play a significant role in cosmic evolution of structures in the Universe. Effects of SMBH feedback or AGN feedback have been directly observed in galaxies and clusters using multi-wavelength datasets (e.g., Roychowdhury 2007; Kormendy & Ho 2013; Fiore et al. 2017; Schellenberger et al. 2017; Harrison 2017; Schutte et al. 2019; Roy et al. 2021a,b). The effect of SMBH feedback on several observables has been explored in the literature, including the $L_x - T$ relation in galaxy clusters and groups (e.g. Puchwein et al. 2010; Andersson et al. 2009; Maughan et al. 2012; Molham et al. 2020), absence of cooling flow in galaxy clusters (e.g., David et al. 2001; Peterson et al. 2003), Sunyaev-Zeldovich (SZ; Sunyaev & Zeldovich 1972) profiles (e.g., Chatterjee et al. 2008), SZ power spectrum (e.g., Chatterjee & Kosowsky 2007; Scannapieco et al. 2008), and star-formation properties of galaxies (e.g., Hopkins et al. 2006; Vitale et al. 2013; Costa et al. 2015; Harrison 2017). In the literature, AGN feedback has been broadly divided into two main modes. The scenario where a very strong quasar outburst launches hot winds in short timescales, is generally classified as the "quasar" or the "radiative" mode while comparatively lower power outflows arising from jets or relativistic plasma which operate on much longer timescales, are classified as "radio" or "kinetic" mode. Hence the radiative mode and the kinetic mode are mostly driven by RQ and RL quasars. However, the specific or distinct roles that these modes play in the evolution of the host galaxy, are still unclear.

As proposed before, an effective way to detect hot outflows can be the SZ effect (Natarajan & Sigurdsson 1999; Aghanim et al. 1999; Yamada et al. 1999; Lapi et al. 2003; Platania et al. 2002; Roychowdhury et al. 2005; Chatterjee & Kosowsky 2007; Scannapieco et al. 2008; Chatterjee et al. 2008; Zanni et al. 2005; Sijacki et al. 2007). The thermal Sunyaev-Zeldovich (tSZ) effect is the spectral distortion of the cosmic microwave background (CMB) radiation arising from the inverse Compton scattering of the CMB photons by the high-energy electrons present along the line of sight (Sunyaev & Zeldovich 1972). The SZ probe is effective in understanding the relative importance of RL and RQ quasars in the evolution of their host galaxies.

1.3. Host Galaxy Property Analysis

One approach to examine whether RL and RQ AGN constitute the same or different populations is to examine the properties of their host galaxies. The hosts of quasars are often star forming galaxies (see review by Heckman & Best 2014a). Star-formation (SF) produces synchrotron radiation from electrons accelerated to relativistic speeds in supernova remnants as well as free-free emission from HII regions (Condon 1992). It has been found that radio continuum emission at low frequencies in low-luminosity quasars is consistent with being dominated by star formation (Gürkan et al. 2019). Further, in contrast with previous studies at lower redshifts (e.g., McLure & Dunlop 2001), Falcke et al. (1996) and Kauffmann et al. (2008) showed that RL AGN appear to be found in denser environments than their RQ counterparts. This is in qualitative agreement with other works on higher redshift quasars as well.

Complex physical interplay between the main baryonic components of galaxies like stars of all ages and their remnants; molecular, atomic, and ionised gas; dust; and supermassive black holes cause multi–wavelength emission spanning from γ–rays to the radio domain. So the typical spectral energy distribution (SED) of a galaxy that covers a broad wavelength range, from X-ray to infrared (IR), contains the imprint of the baryonic processes which drove its formation and evolution along cosmic times. In other words, we need to extract the information tightly woven into the SED of AGN host galaxies across a broad range of redshifts to understand galaxy formation and evolution .

1.4. Summary of Thesis Work

In this thesis work using the quasar catalog from the Sloan Digital Sky Survey (SDSS), we first show that the radio-loud fraction (RLF) for high broad line (HBL) quasars, containing FWHM greater than $15,000$ km s^{-1}, is $\sim 57\%$. We find that there is no significant difference in most of the fundamental properties (except luminosity) between the RL and radio-quiet (RQ) populations in our sample. By comparing them with the non-HBL Hβ broad emission line quasars (sample with FWHM less than $15,000$ km s^{-1}), we find that the HBL sources have the lowest Eddington ratios in addition to having a very high RLF. This is consistent with the theories of jet formation, in which jets are launched from low Eddington ratio accreting systems.

To probe the energetic outflows from quasars that are responsible for heating the intergalactic medium we model the thermal Sunyaev-Zeldovich (SZ) effect from quasar outflows, using the GIZMO meshless finite mass hydrodynamic cosmological simulation SIMBA (Davé et al. 2019). SIMBA includes different prescriptions for quasar feedback namely both the radio loud and the radio quiet modes. From these theoretical simula-

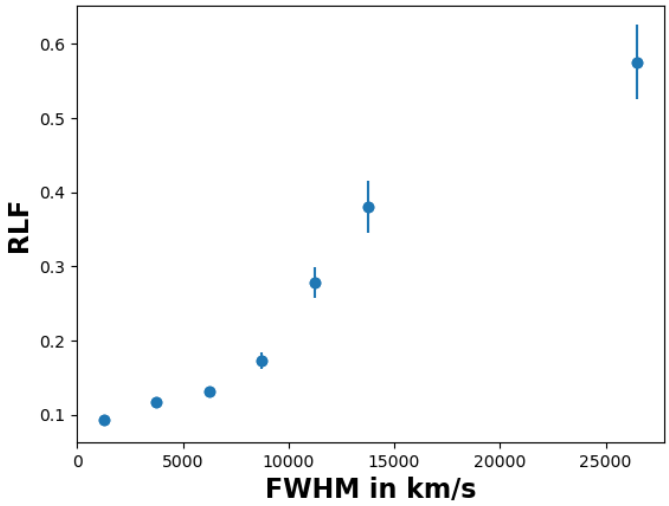

Fig. 1.— Blue dots denote the radio loud fraction (RLF) as a function of FWHM of broad Hβ emission line. The X-axis represents the central value of the FWHM bin. The error-bars used here are binomial errors of the mean value of the RLF. We observe that the RLF increases with FWHM.

tions, we perform mock observations of the Atacama Large Millimeter Array (ALMA) in four bands (320 GHz, 135 GHZ, 100 GHz and 42 GHz) to characterize the feasibility of direct detection of the SZ signal due to outflows from radio loud and radio quiet systems. We note that the radio jet is suppressing the SZ signal significantly and with the current prescription of jet feedback, for the mock maps, the signal goes below the detection threshold of ALMA.

We further investigate the host galaxy properties of radio loud and radio quiet quasars by modeling their spectral energy distribution. Our initial results reveal that the host galaxy properties of RL and RQ quasars are not significantly different.

2. Radio Dichotomy Analysis of Broad Emission Line Quasars

Since the very first discovery of quasars (Schmidt 1963), the radio bi-modality of the quasar population has been discussed in the literature (e.g., White et al. 2000; Brotherton et al. 2001; Lacy et al. 2001; Cirasuolo et al. 2003b,a; Doi et al. 2013; Tadhunter 2016; Hardcastle & Croston 2020). While the principal difference between the radio-loud (RL) and radio-quiet (RQ) quasars lies in the strength of their radio jets (e.g., Bridle et al.

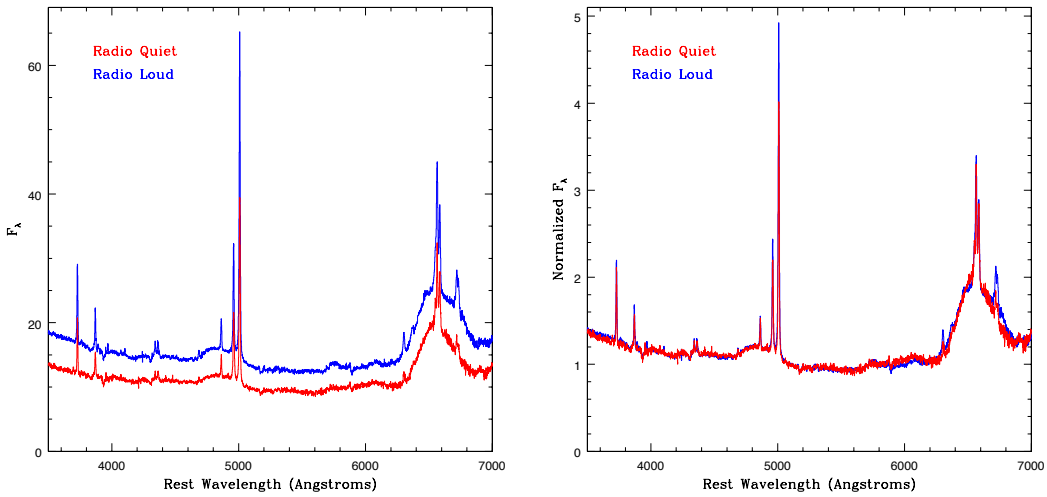

Fig. 2.— **Left Panel:**Combined spectra of RL and RQ quasars with Hβ FWHM greater than 15000 km s^{-1}. F_λ is in the units of $10^{-17} erg/cm^2/s/$Å. **Right Panel:** Normalised combined spectra of RL and RQ quasars with Hβ FWHM greater than 15,000 km s^{-1}, where F_λ is in the units of 10^{-16} erg cm^{-2} s^{-1} Å^{-1}. From the combined spectra we can see that the RL quasars have higher optical continuum flux and stronger [O III] line.

1994; Mullin et al. 2008), several studies have been undertaken to address the source of this dichotomy (e.g., Kellermann et al. 1989; Miller et al. 1990; White et al. 2000; Lacy et al. 2001; Ivezić et al. 2002; White et al. 2007; Laor & Behar 2008; Zamfir et al. 2008; Baloković et al. 2012; Zhang et al. 2021) but we are yet to get the answer.

2.1. Data Sets

In this study we use RL and RQ quasars from Shen et al. (2011), which is the complete quasar catalog obtained from SDSS DR7. The catalog consists of 105, 783 spectroscopically confirmed quasars, that are brighter than $Mi = -22.0$ obtained from a sky coverage of $\sim 9,380 deg^2$. The catalog consists of quasars that have reliable redshifts and have at least one emission line with FWHM greater than 1, 000 km s^{-1}. The flux limit for the main spectroscopic sample is $i < 19.1$.

Shen et al. (2011) use a specific criterion to cross-match the DR7 quasars with the Faint Images of the Radio Sky at Twenty-Centimetres (FIRST) which is a radio survey (White et al. 2007) that scanned over 10,000 square degrees of the North and South Galactic Caps at 1.4 GHz to include radio properties. Out of all 105,783 quasars in

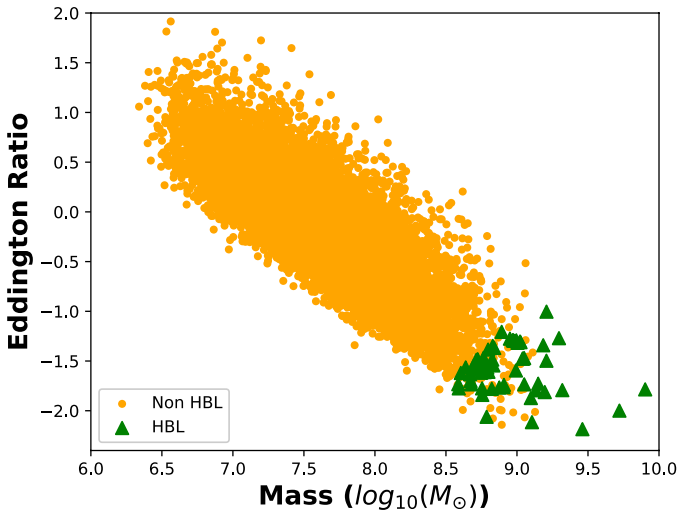

Fig. 3.— Yellow filled circles and green filled triangles show the variation of Eddington ratio with BH mass of quasars with Hβ FWHM greater and less than 15,000 km s^{-1}, i.e., non-HBL and HBL, respectively. As we know that the Eddington ratio is inversely related to the BH mass, we note that our HBL sample contains the quasars with the highest BH mass and the lowest Eddington ratios.

SDSS, 99,182 have a FIRST match. Among those, 9,399 are identified as RL and 88,979 as RQ quasars. We have taken a redshift ($z < 0.75$ for Hβ and $z < 1.9$ for MgII) limited sample (Richards & Kratzer 2014). Our final sample contains 298 RL and 1,910 RQ quasars. Among RL quasars, 56 and 14 have high broad line (FWHM $>$ 15000 kms^{-1}) and in RQ quasars, 41 and 22 have high broad line sources in Hβ and MgII respectively.

Table 1: Correlation Matrix for RL quasars of Hβ HBL Sample

	L_{Bol}	BH mass	FWHM
L_{Bol}	1.0000	0.6855	0.0829
BH mass	0.6855	1.0000	0.7757
FWHM	0.0829	0.7757	1.0000

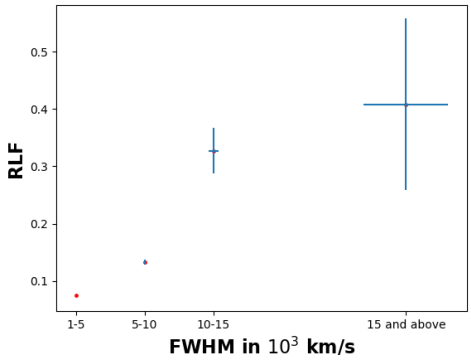

Fig. 4.— Blue dots denote the radio loud fraction (RLF) as a function of FWHM of broad MgII emission line. The x-axis represents the central value of the FWHM bin. The error-bars used here are binomial errors of the mean value of the RLF. We see that the RLF increases with FWHM.

Table 2: Correlation Matrix for RQ quasars of Hβ HBL Sample

	L_{Bol}	BH mass	FWHM
L_{Bol}	1.0000	0.5352	-0.1464
BH mass	0.5352	1.0000	0.7486
FWHM	-0.1464	0.7486	1.0000

2.2. High Broad Emission Line (HBL) Hβ Sample

For broad Hβ emission line quasars, we obtained the variation of radio loud fraction (RLF) with FWHM. Figure 1 clearly exhibits an increasing trend of RLF with the RLF reaching ∼57% in the highest FWHM bin (Chakraborty & Bhattacharjee 2020; Chakraborty et al. 2022). Additionally we found the correlation coefficient to be 0.97 with a p-value 0.0002, implying only a 0.02% chance of finding such high value of the correlation coefficient by chance if the data were not correlated. To investigate this phenomenon in more detail, particularly at the very high end of the Hβ FWHM values, we analyse the properties of RL and RQ quasars with Hβ FWHM greater than $15,000$ km s^{-1} (high broad line or HBL).

Except for the bolometric and optical continuum luminosity, other fundamental properties of RL and RQ HBL quasars like black hole (BH) mass (R_{Fe} corrected), accretion rate, Eddington ratio, covering fraction, and redshift distributions are consistent with each other. Luminosities are slightly higher for RL than RQ. We also found a

correlation between radio luminosity at 6 cm ($L_{\rm rad}$) and optical continuum luminosity at 5100 Å($L_{5100\mathring{A}}$) such that a linear regression relation may be obtained given by $L_{rad} = (1.36 \pm 0.30)\, \mathrm{L}_{5100\mathring{A}} - (28.89 \pm 13.58)$ with a correlation coefficient of 0.62. Hence, we conclude that the accretion disc luminosity of the RL quasars in our HBL sample is higher, which indicates a connection between a brighter disc and a more prominent jet.

Table 3: Correlation Matrix for RL quasars of MgII VBL Sample

	L_{Bol}	BH mass	FWHM
L_{Bol}	1.0000	0.5922	0.2666
BH mass	0.5922	1.0000	0.5766
FWHM	0.2666	0.5766	1.0000

Table 4: Correlation Matrix for RQ quasars of MgII VBL Sample

	L_{Bol}	BH mass	FWHM
L_{Bol}	1.0000	0.8713	-0.0095
BH mass	0.8713	1.0000	0.1304
FWHM	-0.0095	0.1304	1.0000

We compute the composite spectra (Figure 2) of RL and RQ quasars of our HBL sample. From the normalised composite spectra (Figure 2, right) we observe that one of the major differences between the combined spectra of RL and RQ quasars is in the strength of the [O III] narrow line (equivalent width for RL is 42.9 ± 0.1 and for RQ is 41.7 ± 0.2) while the Hβ broad lines are identical for both the samples. So the difference 1.2 and error associated with the difference is 22% (less than 1-σ). We checked that these effects are physical effects and not driven by the most massive sources.

We also perform correlation studies between bolometric luminosity, FWHM, and BH mass of our HBL sample. The results are summarized in Tables 1 and 2. In our sample we observe that bolometric luminosity is not correlated with FWHM (p-value for RL and RQ are 0.15 and 0.39 respectively) but BH mass is correlated with FWHM (p-value 0.0001 for both RL and RQ) as well as bolometric luminosity (p-value for RL and RQ are 0.0001 and 0.0004). Both FWHM and bolometric luminosity increase with BH mass for both our RL and RQ quasar samples. As evident from the tables, the correlation between bolometric luminosity and BH mass is slightly stronger in RL quasars compared to the RQ ones.

We further compare our HBL sample with quasars from the non-HBL sample (FWHM less than $15,000$ km s^{-1}). We compare mass versus Eddington ratio, Eddington ratio versus optical continuum luminosity, and the FWHM versus R_{Fe}, relations respectively,

of both the samples of interest. We find that quasars in our HBL sample has the highest BH mass and lowest Eddington ratios (Figure 3) and optical continuum luminosities compared to the non-HBL sample. We also observe that our HBL sample has the lowest R_{Fe}. For the entire sample we found R_{Fe} to be decreasing with FWHM, consistent with previous studies (Zamfir et al. 2008; Shen & Ho 2014).

2.3. Low Broad Emission Line (LBL) Hβ Sample

We also have analysed the fundamental properties like bolometric luminosity, optical continuum luminosity at 5100Å, BH mass and accretion rate for the RL quasars and RQ quasars with Hβ FWHM less than 2500 km s^{-1} and calling it low broad line (LBL) sample to compare with our HBL sample. We see that the distributions are almost identical for all the properties.

Table 5: Different Feedback Modes

Feedback mode	Configuration
All feedback	Radiative+jet+X-ray
No-jet feedback	Radiative
No X-ray feedback	Radiative+jet

2.4. Very Broad Emission Line (VBL) MgII Sample

SDSS DR7 catalogue includes line fits with multiple Gaussian and contains all the BH masses for the broad Hβ and broad MgII lines quasars. To have a better understanding on the radio dichotomy, after investigating the broad Hβ emission line quasars we also check the variation of radio-loud fraction across FWHM for MgII emission line where we can include higher redshift quasars. From Figure 4 we note that the radio-loud fraction (RLF) is increasing with FWHM similar to Hβ. We find the RLF to be about 40% at very broad line region which implies that very broad line region RL quasars are more in number (Chakraborty & Bhattacharjee 2020). To investigate this phenomenon in more detail, particularly at the very high end of the MgII FWHM values, we analyse the properties of RL and RQ quasars with MgII FWHM greater than $15,000$ km s^{-1} (very broad line or VBL).

We have analysed the fundamental properties like bolometric luminosity, BH mass, optical continuum luminosity and accretion rate of RL quasars and RQ quasars for very

broad line region for MgII. We observe that for all the properties RL quasars have slightly higher values when compared to RQ quasars but covering fraction and redshift distributions are consistent (Chakraborty et al. 2021) whereas in Hβ sample BH mass and accretion rates are also consistent. We have also found a correlation between optical continuum luminosity with BH mass.

We further perform a correlation analyses between bolometric luminosity, BH mass, and FWHM of our VBL RL and RQ quasars and Tables 3 and 4 list the correlation coefficients. We observe in our sample that bolometric luminosity is not correlated with FWHM for both RL and RQ quasars however bolometric luminosity correlates with black hole mass for both RL and RQ quasars. Our analysis suggests that the correlation between bolometric luminosity and BH mass is stronger in RQ quasars compared to the RL ones. Lastly, we observe a modest correlation between BH mass and FWHM for our RL sample. We however wish to note that our results are based on small sample statistics, namely 14 RL and 22 RQ quasars.

We see that for RL quasars, correlation is better between BH mass with bolometric luminosity and FWHM in Hβ HBL sample than MgII VBL sample but bolometric luminosity and FWHM has a better correlation in MgII VBL sample. For RQ quasars, we see a better correlation between FWHM with bolometric luminosity and BH mass in Hβ HBL sample than MgII VBL sample but bolometric luminosity and BH mass has a better correlation in MgII VBL sample.

3. The Sunyaev-Zeldovich Effect from Quasar Feedback

After analysing the AGN properties we investigate the effect of AGN outflow in the surrounding intergalactic medium. As previously discussed, we use the SZ signal to probe the AGN feedback. For this work, we have used the SIMBA simulation (Davé et al. 2019). SIMBA is one of the most updated cosmological simulations which is the next generation of the MUFASA cosmological galaxy formation simulations that runs with GIZMO's meshless finite mass hydrodynamics with different feedback prescriptions (Table 5).

3.1. Modelling Feedback Modes from Active Galactic Nuclei

The black holes (BHs) are seeded and considered to be collisionless sink particles, which can grow by accreting the surrounding gas or by merging with other BHs. The accretion rate of the BHs is modelled via two processes, one is torque-limited accretion model (Anglés-Alcázar et al. 2017) and the other is the Bondi accretion model (Bondi

Table 6: CASA Parameters for 'simalma'

Parameters	Values
incell	0.5 arcsec
incenter	320 GHz/135 GHz/100 GHz/42 GHz
inwidth	7.5 GHz
integration	30s
mapsize	10 arcsecs
antennalist	alma.cycle 8.1.cfg
totaltime	3h
pwv	0.5
imsize	300
cell	0.1 arcsec/0.23 arcsec/0.32 arcsec/0.76 arcsec
niter	1000

1952; Hoyle & Lyttleton 1939).

A kinetic subgrid model has been incorporated for black hole feedback along with X-ray energy feedback. The motivation for the kinetic feedback model comes from the observed dichotomy which includes a "radiative mode" at high Eddington ratios and a "jet mode" at low Eddington ratios in black hole growth modes that is reflected in their outflow characteristics (e.g., Heckman & Best 2014b). Apart from kinetic feedback, energy input into surrounding gas for the photoionization heating from the X-ray photons coming from the accretion disk of the AGN is also included (Choi et al. 2012).

3.2. Construction of Sunyaev-Zeldovich Maps

To perform our analysis we have made use of the SIMBA halo catalog and selected two representative black holes from the simulation, the most massive (highest mass) and the most active (highest accretion rate) ones at z= 0.016 and z= 1.0. To obtain the SZ map around the black holes, a projected direction is chosen and then the SZ signal arising from all the elements along the line of sight is integrated for all the pixels in the map. The change in the intensity of the CMB due to the tSZ effect is given by Sazonov & Sunyaev (1998) :

$$\Delta I(x) = \frac{2k_B T_{CMB}}{\lambda^2} \frac{x^2 e^x}{(e^x - 1)^2} \frac{k_B \sigma_T}{m_e c^2} f_1(x) \int \mathrm{d}l \, n_e(l) T_e(l) \tag{1}$$

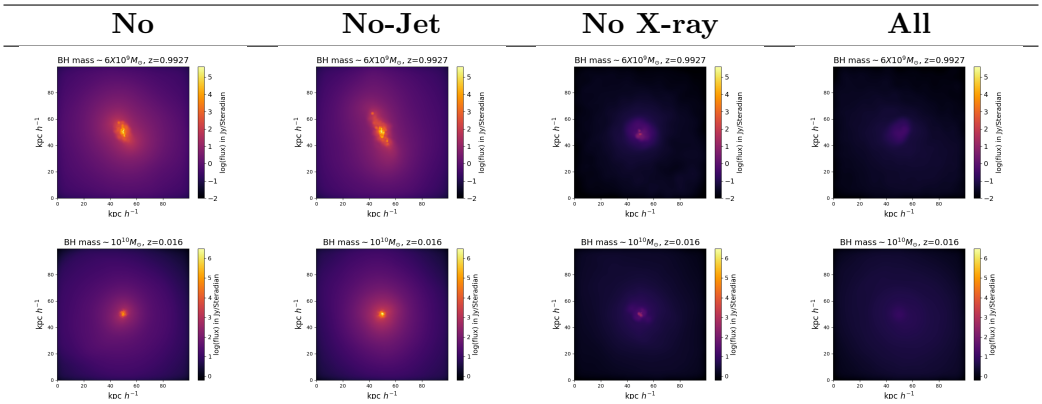

Fig. 5.— The theoretical simulated tSZ maps for different feedback modes (left most: no feedback, second left: no jet feedback, second right: no X-ray feedabk, rightmost: all feedback) around similar BHs at z∼1 from Davé et al. (2019). **Top Panel** Simulated tSZ map at 320 GHz of the most massive black hole for no feedback, no jet feedback, no X-ray feedback and all feedback modes respectively. **Bottom Panel** Same as the top panel but now at $z = 0.016$. From the figure we see that addition of radiative feedback and jet feedback have opposing effects (enhancement versus decrement) in the SZ signal.

where $x = h\nu/(k_B T_{CMB})$, and the integral is along the line of sight direction specified by the direction of projection and $f_1(x) = x\coth(x/2) - 4$ stands for the frequency dependence of the tSZ effect. n_e and T_e are the electron number density and temperature along the line-of-sight.

3.3. Theoretical Sunyaev-Zeldovich Maps

Figure 5 shows the simulated tSZ maps (500×500 pixels) at 320 GHz for different feedback modes around the most massive BHs (identified in the simulations) in a 100 square h^{-1}kpc region at z∼1 and $z = 0.016$. Here we compare tSZ signal for different feedback modes, namely no feedback, no-jet feedback, no X-ray feedback, and all feedback. For both cases tSZ signal is the lowest for all feedback mode, and the suppression of the signal is driven by the jet mode of feedback. The SZ signal gets enhanced for the no-jet feedback (radiative feedback only) case compared to the no-feedback model. Most active BHs follow the similar trend as well. Similar results are obtained from the radial profiles.

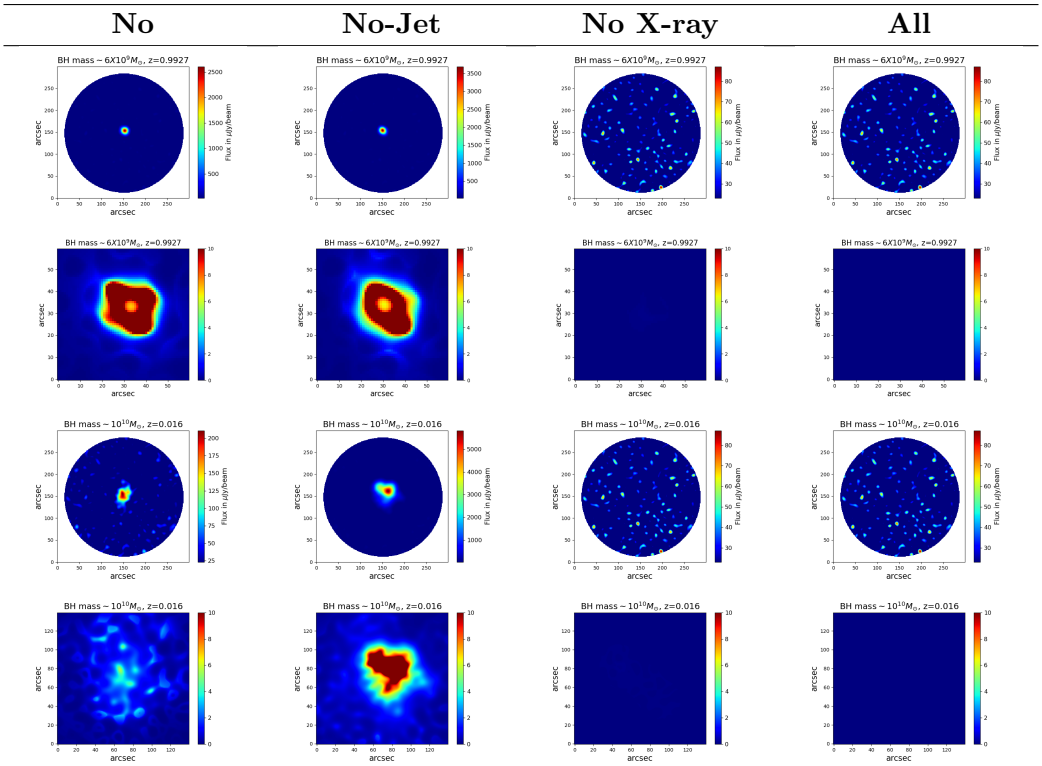

Fig. 6.— The mock ALMA tSZ maps at 320 GHz (Band 7) for different feedback modes around most massive and corresponding signal to noise maps at two different redshifts from (Davé et al. 2019) using the observational parameters in Table 6. **Top Panel** The mock ALMA tSZ maps for no feedback (**left most column**), no-jet feedback, no X-ray feedback, and all feedback modes (**right most column**) respectively around the most massive BH at z∼1. **Second Panel** The corresponding signal-to-noise maps. **Third Panel** Same as the top panel but now at z=0.016. **Fourth Panel** The corresponding signal-to-noise maps. We note that ALMA has the capability to detect the SZ signal for the no feedback and no-jet feedback modes. The signal gets enhanced when, only the radiative mode of feedback is added. For no X-ray feedback and all feedback modes the signal gets suppressed below the noise threshold of ALMA.

3.4. Mock Observational SZ Maps

Figure 6 shows the simulated ALMA maps of the most massive BHS constructed using the observing parameters shown in Table 6 where the minimum flux of the maps is set to the rms value of the noise. The maps are made at 320 GHz (Band 7). The second and the fourth columns represent corresponding signal-to-noise maps of the first and third column.

From Figure 6 we note that once the jet mode of feedback is turned on, the SZ signal drops significantly and goes below the detection threshold of ALMA. It is also seen that for all systems, the signal is most prominent when the radiative mode of feedback is turned on. We got similar results from the most active BHs as well. Also the signal is more pronounced at higher redshifts for both set of BHs. ALMA observations may serve as important probes in understanding feedback effects at higher redshifts as well as constraining theoretical models of feedback. We also check for the simulated ALMA maps constructed using the same observing parameters as Figure 6 at other three lower frequency bands such as 135 GHz (Band 4), 100 GHz (Band 3), and 42 GHz (Band 1). Results are summarized in Table 7. We note that for all cases , turning on the jet feedback suppresses the signal below the ALMA detection threshold and hence we have only included the no-feedback and the radiative feedback simulations for the lower frequency bands.

4. Spectral Energy Distribution Analysis of the Quasar Sample

Modelling the SED of AGN host galaxies is an intricate problem as it involves AGN contribution as well. Galaxies with very different properties can have broadly similar SEDs and misinterpretation of the SED could lead to unrealistic physical properties. This is particularly the case when a partial SED is considered, which is available at restricted wavelength ranges. Therefore, estimating the physical properties of galaxies precisely and accurately, is a considerable challenge with only limited data. In practice, to build physically motivated SED models and attempt to determine their intrinsic physical properties, different techniques are used.

4.1. The Code: X-CIGALE

The `X-CIGALE` code (Yang et al. 2020) is a modular code written in the Python language whose purpose is to model the spectra of galaxies from FUV to radio wavelengths. Based on the earlier `CIGALE` code (Boquien et al. 2019) it can also estimate the physical

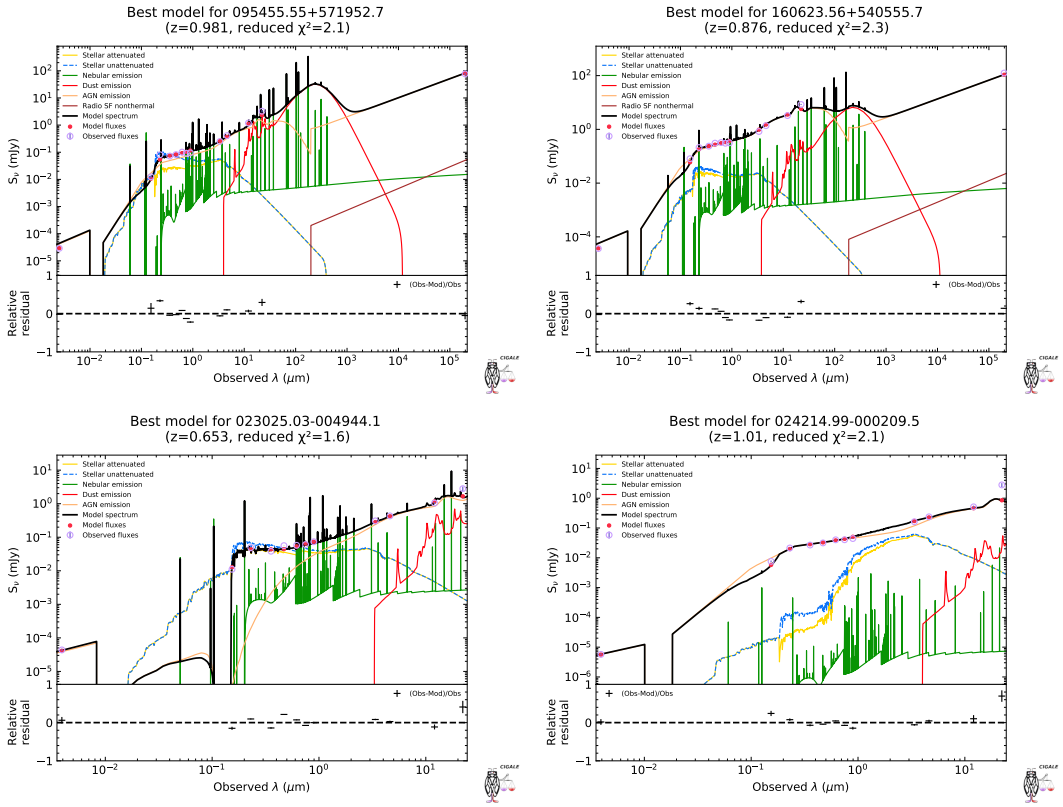

Fig. 7.— Examples of SEDs from radio-loud and radio quiet quasars sources used in our analysis constructed by the X-CIGALE code. χ^2 values calculated by X-CIGALE code for individual SEDS are provided in the plots.

properties of a galaxy, for example, star formation rate (SFR), total stellar mass in the galaxy, contribution of dust luminosity, etc.

For this work we cross-matched our Hβ RL and RQ sample with WISE, GALEX and X-ray data. So our sample have five detections (u, g, r, i, and z photometric bands of SDSS) in optical band, four detections (W1, W2, W3, W4 band of WISE) in infrared band, two UV detections (FUV and NUV band of GALEX), and one X-ray detection (Chandra/ROSAT/Swift/XMM) with their respective errors. In addition to that our RL sample has one radio detection (FIRST 1.4 GHz band). Shen et al. (2011) did not include error for FIRST detections so we have assumed 10% error. SED fitting using X-CIGALE depends on the input parameter values and choice of models. Figure 7 represent some examples of SED from RL and RQ sources used in our analysis.

5. Summary of Results and Future Plans

In this work we show that the radio loud fraction increases with the FWHM of broad Hβ and MgII emission line quasars identified in the SDSS. To further investigate this effect, we selected a subsample of extreme objects (FWHM $>$ 15,000 km s^{-1}) to study their properties in detail. For both Hβ and MgII sample we did not see significant difference in the extreme RL and RQ quasar properties. On the other hand, we note that for Hβ, the BH mass of the quasars in our subsample are, on average, higher than that of the non-HBL SDSS quasars while the Eddington ratios of the quasars in our subsample $\sim 10^{-2} - 10^{-1}$, are significantly lower than the average of that of the non-HBL quasars which is in agreement with jet formation theory. We observe that given the difference in the bolometric or optical continuum luminosity is mainly due to that of the accretion disk, the above implies some connection between a stronger jet and a brighter disk.

To understand the implication of these outflows on the thermodynamics of the inter-galactic/intra-cluster medium we perform theoretical modeling of the effect of these outflows usisng cosmological hydrodynamic simulations. We particularly focus on the Sunyaev-Zeldovich effect which is emerging as a state-of-the-art cosmological tool for studying baryonic physics. From our SZ effect study, as discussed before, we find that once the radiative feedback (wind mode) is modeled, the SZ signal gets enhanced while the inclusion of the jet mode of feedback drastically suppresses the SZ signal and it goes below the detection threshold of the Atacama Large Millimeter Array, which is currently the best observational probe for sub-mm signals. Our analysis provides an upper limit on the amount of feedback that is allowed to model in simulations from SZ observables. By comparing the SZ signal at different frequencies, we note that the lower frequency bands capture more of the signal on large angular scales, particularly important for our low redshift simulation. We further note that due to the nature of SZ signal (its redshift independence) it gets better detected at higher redshifts, at which the quasars are more active.

My future research plan is to investigate the impact of AGN outflows on their host galaxy properties (e.g., stellar population age, stellar mass, star formation rate (SFR)) through spectral energy distribution (SED) analysis using the X-CIGALE code. It calculates the SED likelihood for each set of input parameters and determine the best-fit model and calculates host galaxy properties for that model. Our preliminary SED work has led to two successful observing proposals, namely with AstroSat and Effelsberg proposal. For the Astrosat program (A11_047: PI Avinanda Chakraborty) the observations are complete. I am currently performing the data analysis and the modeling. For the Effelsberg 100m radio telescope proposal (Code: 93-21, PI: Avinanda Chakraborty), the

observation runs are complete and the majority of our sources have been detected at two radio frequencies. The next steps are the reduction, calibration and analysis of our data respectively.

Acknowledgement

I would like to first thank my supervisor, Dr.Suchetana Chatterjee, for all the support, help, guidance and patience. I am indebted to her for showing faith on me and motivating me. I would also like to thank all my colleagues, co-authors, juniors and seniors who played significant roles in my life and research. I acknowledge financial support from the Department of Science and Technology through the SERB-ECR grant, and SERB-CRG grant of Dr.Suchetana Chatterjee.

REFERENCES

Aghanim, N., Desert, F. X., Puget, J. L., & Gispert, R. 1999, A&A, 341, 640

Andersson, K., Peterson, J. R., Madejski, G., & Goobar, A. 2009, ApJ, 696, 1029

Anglés-Alcázar, D., Davé, R., Faucher-Giguère, C.-A., Özel, F., & Hopkins, P. F. 2017, MNRAS, 464, 2840

Baloković, M., Smolčić, V., Ivezić, Ž., Zamorani, G., Schinnerer, E., & Kelly, B. C. 2012, ApJ, 759, 30

Blandford, R. D. 1990, in Active Galactic Nuclei, ed. R. D. Blandford, H. Netzer, L. Woltjer, T. J. L. Courvoisier, & M. Mayor, 161

Blandford, R. D., & Znajek, R. L. 1977, MNRAS, 179, 433

Bondi, H. 1952, MNRAS, 112, 195

Boquien, M., Burgarella, D., Roehlly, Y., Buat, V., Ciesla, L., Corre, D., Inoue, A. K., & Salas, H. 2019, A&A, 622, A103

Bridle, A. H., Hough, D. H., Lonsdale, C. J., Burns, J. O., & Laing, R. A. 1994, AJ, 108, 766

Brotherton, M. S., Tran, H. D., Becker, R. H., Gregg, M. D., Laurent-Muehleisen, S. A., & White, R. L. 2001, ApJ, 546, 775

Chakraborty, A., & Bhattacharjee, A. 2020, arXiv e-prints, arXiv:2011.08630

Chakraborty, A., Bhattacharjee, A., Brotherton, M. S., Chatterjee, R., Chatterjee, S., & Gilbert, M. 2022, MNRAS, 516, 2824

Chakraborty, A., Bhattacharjee, A., & Chatterjee, S. 2021, Galaxies, 9, 74

Chatterjee, S., Di Matteo, T., Kosowsky, A., & Pelupessy, I. 2008, MNRAS, 390, 535

Chatterjee, S., & Kosowsky, A. 2007, ApJ, 661, L113

Choi, E., Ostriker, J. P., Naab, T., & Johansson, P. H. 2012, ApJ, 754, 125

Cirasuolo, M., Celotti, A., Magliocchetti, M., & Danese, L. 2003a, MNRAS, 346, 447

Cirasuolo, M., Magliocchetti, M., Celotti, A., & Danese, L. 2003b, MNRAS, 341, 993

Condon, J. J. 1992, ARA&A, 30, 575

Costa, T., Sijacki, D., & Haehnelt, M. G. 2015, MNRAS, 448, L30

Davé, R., Anglés-Alcázar, D., Narayanan, D., Li, Q., Rafieferantsoa, M. H., & Appleby, S. 2019, Monthly Notices of the Royal Astronomical Society, 486, 2827–2849

David, L. P., Nulsen, P. E. J., McNamara, B. R., Forman, W., Jones, C., Ponman, T., Robertson, B., & Wise, M. 2001, ApJ, 557, 546

Doi, A., Asada, K., Fujisawa, K., Nagai, H., Hagiwara, Y., Wajima, K., & Inoue, M. 2013, ApJ, 765, 69

Falcke, H., Sherwood, W., & Patnaik, A. R. 1996, ApJ, 471, 106

Fiore, F., et al. 2017, A&A, 601, A143

Franceschini, A., Vercellone, S., & Fabian, A. C. 1998, MNRAS, 297, 817

Garofalo, D., Evans, D. A., & Sambruna, R. M. 2010, MNRAS, 406, 975

Gürkan, G., et al. 2019, A&A, 622, A11

Hamilton, T. S. 2010, MNRAS, 407, 2393

Hardcastle, M. J., & Croston, J. H. 2020, , 88, 101539

Harrison, C. M. 2017, Nature Astronomy, 1, 0165

Heckman, T. M., & Best, P. N. 2014a, ARA&A, 52, 589

Heckman, T. M., & Best, P. N. 2014b, ARA&A, 52, 589

Hickox, R. C., et al. 2009, ApJ, 696, 891

Hopkins, P. F., Robertson, B., Krause, E., Hernquist, L., & Cox, T. J. 2006, ApJ, 652, 107

Hoyle, F., & Lyttleton, R. A. 1939, Proceedings of the Cambridge Philosophical Society, 35, 405

Hughes, S. A., & Blandford, R. D. 2003, ApJ, 585, L101

Ivezić, Ž., et al. 2002, AJ, 124, 2364

Kauffmann, G., Heckman, T. M., & Best, P. N. 2008, MNRAS, 384, 953

Kellermann, K. I., Sramek, R., Schmidt, M., Shaffer, D. B., & Green, R. 1989, AJ, 98, 1195

Kimball, A. E., Kellermann, K. I., Condon, J. J., Ivezić, Ž., & Perley, R. A. 2011, ApJ, 739, L29

Kormendy, J., & Ho, L. C. 2013, ARA&A, 51, 511

Lacy, M., Laurent-Muehleisen, S. A., Ridgway, S. E., Becker, R. H., & White, R. L. 2001, ApJ, 551, L17

Lagos, C. D. P., Padilla, N. D., & Cora, S. A. 2009, MNRAS, 395, 625

Laor, A., & Behar, E. 2008, MNRAS, 390, 847

Lapi, A., Cavaliere, A., & De Zotti, G. 2003, ApJ, 597, L93

Maughan, B. J., Giles, P. A., Randall, S. W., Jones, C., & Forman, W. R. 2012, MNRAS, 421, 1583

McLure, R. J., & Dunlop, J. S. 2001, Monthly Notices of the Royal Astronomical Society, 321, 515

McLure, R. J., & Jarvis, M. J. 2004, MNRAS, 353, L45

McLure, R. J., Kukula, M. J., Dunlop, J. S., Baum, S. A., O'Dea, C. P., & Hughes, D. H. 1999, MNRAS, 308, 377

Miller, L., Peacock, J. A., & Mead, A. R. G. 1990, MNRAS, 244, 207

Molham, M., et al. 2020, MNRAS, 494, 161

Mullin, L. M., Riley, J. M., & Hardcastle, M. J. 2008, MNRAS, 390, 595

Natarajan, P., & Sigurdsson, S. 1999, MNRAS, 302, 288

Peterson, J. R., Kahn, S. M., Paerels, F. B. S., Kaastra, J. S., Tamura, T., Bleeker, J. A. M., Ferrigno, C., & Jernigan, J. G. 2003, ApJ, 590, 207

Platania, P., Burigana, C., De Zotti, G., Lazzaro, E., & Bersanelli, M. 2002, MNRAS, 337, 242

Puchwein, E., Springel, V., Sijacki, D., & Dolag, K. 2010, MNRAS, 406, 936

Richards, G. T., & Kratzer, R. 2014, in American Astronomical Society Meeting Abstracts, Vol. 223, American Astronomical Society Meeting Abstracts #223, 150.35

Roy, N., et al. 2021a, ApJ, 913, 33

Roy, N., et al. 2021b, ApJ, 922, 230

Roychowdhury, S. 2007, in Groups of Galaxies in the Nearby Universe, ed. I. Saviane, V. D. Ivanov, & J. Borissova, 337

Roychowdhury, S., Ruszkowski, M., & Nath, B. B. 2005, ApJ, 634, 90

Sabater, J., et al. 2019, A&A, 622, A17

Sazonov, S. Y., & Sunyaev, R. A. 1998, Astronomy Letters, 24, 553

Scannapieco, E., Thacker, R. J., & Couchman, H. M. P. 2008, ApJ, 678, 674

Schellenberger, G., Vrtilek, J. M., David, L., O'Sullivan, E., Giacintucci, S., Johnston-Hollitt, M., Duchesne, S. W., & Raychaudhury, S. 2017, The Astrophysical Journal, 845, 84

Schmidt, M. 1963, Nature, 197, 1040

Schutte, Z., Reines, A. E., & Greene, J. E. 2019, ApJ, 887, 245

Shen, Y., & Ho, L. C. 2014, Nature, 513, 210

Shen, Y., Mulchaey, J. S., Raychaudhury, S., Rasmussen, J., & Ponman, T. J. 2007, ApJ, 654, L115

Shen, Y., et al. 2011, ApJS, 194, 45

Sijacki, D., Springel, V., Di Matteo, T., & Hernquist, L. 2007, MNRAS, 380, 877

Sikora, M., Stawarz, Ł., & Lasota, J.-P. 2007, ApJ, 658, 815

Sunyaev, R. A., & Zeldovich, Y. B. 1972, Comments on Astrophysics and Space Physics, 4, 173

Tadhunter, C. 2016, A&A Rev., 24, 10

Vitale, M., et al. 2013, A&A, 556, A11

White, R. L., et al. 2000, ApJS, 126, 133

White, R. L., Helfand, D. J., Becker, R. H., Glikman, E., & de Vries, W. 2007, ApJ, 654, 99

Yamada, M., Sugiyama, N., & Silk, J. 1999, ApJ, 522, 66

Yang, G., et al. 2020, MNRAS, 491, 740

Zamfir, S., Sulentic, J. W., & Marziani, P. 2008, MNRAS, 387, 856

Zanni, C., Murante, G., Bodo, G., Massaglia, S., Rossi, P., & Ferrari, A. 2005, A&A, 429, 399

Zhang, L., Fan, J., & Zhu, J. 2021, Publications of the Astronomical Society of Japan, 73, 313

This preprint was prepared with the AAS LaTeX macros v5.0.

Journal Publications and Conference Proceedings

Refereed Publications

Cosmological Simulation of Galaxy Groups and Clusters-III: Characterizing Quasar Feedback Modes with the Sunyaev-Zeldovich Effect, **A. Chakraborty**, S. Roy, S. Chatterjee, S. Roy, and R. Kar Chowdhury, (under review in **ApJ**), **(2023)**, IF: 5.58

Radio Dichotomy in Quasars with Hβ FWHM greater than 15,000 km s^{-1}, **A. Chakraborty** , A. Bhattacharjee, M. Brotherton, R. Chatterjee, S. Chatterjee, and M. Gilbert, **MNRAS**, 516, 2824 **(2022)**, IF: 5.23

Properties of Very Broad Line MgII Radio-loud and Radio-quiet Quasars, **A. Chakraborty** , A. Bhattacharjee, and S. Chatterjee, **Galaxies**, Special Issue, 9(4), 74, **(2021)**, IF:3.17

BH Mass, Jet And Accretion Disk Connection : An Analysis Of Radio-Loud And Radio-Quiet Quasars, **A. Chakraborty** & A. Bhattacharjee, **Astronomische Nachrichten (AN)**, 342, 142, **(2020)**, IF:1.06

Non-Refereed Publications

Spectroscopic properties of radio-loud and radio-quiet quasars,
A. Chakraborty & A. Bhattacharjee, **Nuclear Activity in Galaxies Across Cosmic Time**, Cambridge University Press, 15(S356), 72, **(2019)**

Science with an ngVLA: The Sunyaev-Zeldovich Effect from Quasar and Starburst Winds, M. Lacy, S. Chatterjee, **A. Chakraborty**, B. Mason, C. Sarazin, A. Kimball, K. Nyland, G. Rocha, & B. Rowe, **ASP Monograph Series**, Vol. 517, Science with a Next-Generation VLA, **(2019)**

Contributed Presentations

1. Contributed Talk, 'Constraining Quasar Feedback Models with the Atacama Large Milimeter Array by Probing Sunyaev-Zel'dovich Signals', Largest Cosmological Surveys and Big Data Science, ICTS, May 1st-12th, **(2023)**

2. Contributed Flash Talk+Poster , "Characterizing Quasar Feedback Modes with the Sunyaev-Zeldovich Effect", 32nd meeting of Indian Association for General Relativity and Gravitation (IAGRG32), Indian Institutes of Science Education and Research (IISER) Kolkata, Kolkata, December 19th - 21st, **(2022)**.

3. Contributed Talk , "Characterizing the Effect of Quasar Feedback in X-ray and Sunyaev-Zel'dovich Signals from Galaxy Clusters", Young Astronomers' Meet (YAM) 2022, Aryabhatta Research Institute of Observational Sciences (ARIES), Nainital, November 9th - 13th, **(2022)**.

4. Contributed Poster (Virtual), "SED Analysis of Broad Emission Line Quasars", Large-Volume Spectroscopic Analyses of AGN and Star Forming Galaxies in the Era of JWST Workshop at STScI, March 29th - April 1st, **(2022)**.

5. Contributed Poster (Virtual), "Host Galaxy Properties Analysis of Broad Emission Line Quasars", Astronomical Society of India, Roorkee, March 25th - 29th, **(2022)**. First-author Maitreya Kundu.

6. Contributed Talk (Virtual), "The radio dichotomy in extreme objects: Stutying quasars with FWHM greater than 15000 km/s", Crimean-2021 AGN Conference: Galaxies with Active Nuclei on Scales from Black Hole to Host Galaxy, Nauchny, September 13th -17th, **(2021)**.

7. Contributed Poster (Virtual), "The radio dichotomy in extreme objects: Stutying quasars with FWHM greater than 15000 km/s", 13th Serbian Conference on Spectral Line Shapes in Astrophysics, Belgrade, Serbia, August 23rd - 27th, **(2021)**.

8. Contributed Lightning Talk (Virtual), "Accretion Disk and Jet Connection: An Analysis of Radio-loud and Radio-quiet Quasars", RGCW 2021- A new window on the radio emission from galaxies, galaxy clusters and cosmic web: current status and perspectives, March 8th - 10th, **(2021)**.

9. Contributed Poster (Virtual), "Studying the SunayevZel'dovich effect and X-ray Emission from Quasar Feedback", Astronomical Society of India , February 18th - 23nd, **(2021)**

10. Contributed Talk (Virtual), "BH Mass, Jet and Accretion Disk Connection: An Analysis of Radio-loud and Radio-quiet Quasars", IWARA 2020 - From Quarks to Cosmos video conference , Mexico, September 6th - 12th, **(2020)**

11. Contributed Poster (Virtual), "Spectroscopic Properties Of Radio-loud (RL) And Radio-quiet (RQ) Quasars", European Astronomical Society Annual Meeting -EAS 2020 (EWASS), Leiden, June 29th - July 3rd, **(2020)**

12. Contributed Poster (Virtual), "Spectroscopic Properties Of High Velocity MgII and H-Beta Emission Lines of Radio Loud And Radio Quiet Quasars", American Astronomical Society-AAS 236, June 1st - 3rd, **(2020)** First-author Anirban Bhattacharjee.

13. Contributed Poster, "Spectroscopic Properties Of Radio Loud And Radio Quiet Quasars", National Seminar on Applications of Statistics in Natural Sciences, St. Xavier's College, Kolkata, December 16th - 17th, **(2019)**

14. Contributed Talk, "Spectroscopic Properties Of High Velocity MgII and H-Beta Emission Lines of Radio Loud And Radio Quiet Quasars", International Astronomical Union - IAU 356, 'Nuclear Activity in Galaxies Across Cosmic Time' symposium, Ethiopia, October 7th - 11th **(2019)**

15. Contributed Poster, "Hβ emission line properties of high velocity quasars and correlation between the origin of radio emission and optical emission", Astronomical Society of India, Bangalore, February 18th-22nd, **(2019)**

Table 7: Summary of Mock ALMA SZ Results

	Mode	z	Band	Beam (arcsec)	SNR Peak	Signal (μJy) Peak
Massive	None	0.99	7	1.04	12	2604.8
			4	2.6	3	-221.5
			3	3.4	6	-234.8
			1	8.2	37	-68.7
		0.016	7	1.04	3	211
			4	2.6	4	-58.3
			3	3.4	4	-91.8
			1	8.2	2	-60.9
	No-Jet	0.99	7	1.04	10	3692.2
			4	2.6	4	-300.3
			3	3.4	5	-316.6
			1	8.2	13	-91.8
		0.016	7	1.04	19	5817.7
			4	2.6	12	-1242.4
			3	3.4	20	-1767.5
			1	8.2	9	-834.4
Active	None	0.99	7	1.04	4	87.3
			4	2.6	1	-24.2
			3	3.4	2	-23.1
			1	8.2	4	-17.9
		0.016	7	1.04	1	86.7
			4	2.6	2	-23.7
			3	3.4	3	-26.9
			1	8.2	2	-18
	No-Jet	0.99	7	1.04	8	290.6
			4	2.6	3	-209.7
			3	3.4	4	-189.3
			1	8.2	20	-53.6
		0.016	7	1.04	1	87.6
			4	2.6	3	-45.6
			3	3.4	5	-49.2
			1	8.2	4	-32.3